Int J Thermophys (2010) 31:805–815
DOI 10.1007/s10765-010-0772-2

Photothermal Radiometry and Diffuse Reflectance Analysis of Thermally Treated Bones

S. Trujillo · P. Martínez-Torres · P. Quintana · Juan Jose Alvarado-Gil

Received: 17 June 2009 / Accepted: 27 May 2010 / Published online: 22 June 2010

Abstract Different fields such as archaeology, biomedicine, forensic science, and pathology involve the analysis of burned bones. In this work, the effects of successive thermal treatments on pig long bones, measured by photothermal radiometry and diffuse reflectance are reported. Measurements were complemented by X-ray diffraction and infrared spectroscopy. Samples were thermally treated for 1 h within the range of 25 °C to 350 °C. The thermal diffusivity and reflectance increase in the low-temperature range, reaching a maximum around 125 °C and decaying at higher temperatures. These results are the consequence of complex modifications occurring in the inorganic and organic bone structure. For lower temperatures dehydration, dehydroxilation, and carbonate loss processes are dominant, followed by collagen denaturing and decompositions, which have an influence on the bone microstructure.

Keywords Diffuse reflectance · FTIR · Heated bones · Photothermal radiometry · Thermal diffusivity · X-ray diffraction

1 Introduction

Bone comprised an organic matrix network (30 %) interwoven with a framework of crystallized mineral matter (70 %), composed primarily of calcium phosphate with a carbonated hydroxyapatite (HA)-like structure, $Ca_{10}(PO_4)_6(OH)_2$. Bioapatite has a range of lattice substitutions and a non-stoichiometric composition. It is known that bony natural apatites contain carbonate ions in a significant amount, from about

S. Trujillo · P. Martínez-Torres · P. Quintana · J. J. Alvarado-Gil (✉)
Depto. de Física Aplicada, CINVESTAV-IPN Unidad Mérida, Antigua Carretera a Progreso km 6, A.P. 73 Cordemex, 97310 Mérida, Yucatán, México
e-mail: jjag@mda.cinvestav.mx; jjag09@yahoo.com

3 mass% up to 8 mass%, which are partially substituted by phosphate ions (PO_4^{3-}) and hydroxide ions (OH^-) [1].

The organic portion is a primary protein component of type I collagen; additionally, there are several non-collagenous proteins, mainly osteocalcin. Collagen is a flexible, tough protein that dictates the shape of the bone, and the mineral crystallites form initially in the collagen fibril, generally oriented along the long axis of the bone. The HA phase is bonded by functional polar groups on the protein molecules and provides additional strength [2]. The mineralized fibers are then packed into lamallae, which in an osteonal bone show a rotated plywood architecture of concentric rings, surrounding the central Haversian canal. In this way, crystallization of bone obeys a hierarchical organization from the nanoscale to the macroscale.

The analysis of burned osteological materials is a topic of interest for scientists in biomaterials, forensic, archaeological, and paleontological fields. Different methodologies have been devised providing interesting results using infrared thermography, Fourier transform infrared spectroscopy (FTIR), and X-ray diffraction (XRD) [1–5].

Thermophysical analysis of bones has been demonstrated to be useful for various biomedical applications, as deproteination is induced by heating at 200 °C and 500 °C for bone transplantation [6,7]. The effect of heating due to a high power laser has increasing interest in bone drilling, and is useful in surgery [8]. It is relevant in the treatment of otosclerosis [9]. Bone heating efficiency has also been evaluated in the treatment of hyperthermia when magnetic nanoparticles of HA are used [10]. Additionally, in spite of these applications, little is known of the precise nature of the physicochemical changes and microstructural nature of bone upon heating at low temperatures, around 200 °C and 600 °C. Therefore, it is necessary to perform further investigations of the thermal and optical properties of intact and thermally treated bones, using complementary analytical methods capable of providing a deeper understanding of the underlying phenomena.

Optical characterization is useful in the detection of a variety of medical and forensic conditions, in the analysis of degradation by different factors, particularly aging, burning, staining of forensic bone [11], in bone demineralization studies [12], and in the effect of impregnation clearing agents on bone surfaces [13], among others. Optical spectroscopy is based on the response of a material to light. It is a highly sensitive methodology that depends on the coupling of light to matter, and for this reason, it represents a simple, non-destructive, and low-noise technique. In the particular case of biological materials, reflectance measurements and its extended approaches have been used successfully even in those cases in which the materials are highly light dispersive [14–17]. Photothermal radiometry (PTR) is a non-contact and non-destructive characterization method, which has been applied successfully to determine the thermal properties in a great variety of materials such as ceramic coatings [18], layered materials [19], in the inspection of solid foods (fresh vegetables and fruits) [20], thermally treated steels [21], nanoparticles and live bio-tissues for medical purposes [22–24], etc.

In this article, PTR and diffuse reflectance are used to analyze thermally treated bones. It is shown that the thermal diffusivity and optical reflectance increase in the low-temperature range, reaching a maximum around 125 °C and decaying at higher temperatures. Our analyses are complemented by FTIR spectroscopy and XRD.

The relationship of the thermal diffusivity and optical reflectance with the chemical milieu and the microstructural changes of the organic matter due to the heating effect are discussed.

2 Materials and Methods

2.1 Sample Preparation and Characterization

Dried pig bones from the central part of the diaphysis of approximately 5 cm height were sliced in a longitudinal section of 1 cm × 1 cm using a Dremel® drill. Afterward, they were polished with water sandpaper (No. 400 and 600) to remove the trabecular and cortical external bone layers from both sides to achieve smooth and flat thin samples (from 200 μm up to 300 μm thickness), appropriate for optical and photothermal measurements. Bone samples were placed into ceramic crucibles and put into a preheated electric furnace for 1 h at a fixed temperature. The same sample was subsequently heated at higher temperatures, in the range from room temperature up to 350 °C.

X-ray diffraction patterns were obtained with a Siemens D5000, CuKα radiation, operating at 34 kV and 25 mA. The specimens were registered in a zero background holder to avoid external background interferences in the range of $15° \leq 2\theta \leq 65°$, in a step scan mode of 2° (2θ) and a counting time of 12 s per step. IR spectra were recorded on bone powder samples (5 mg) mixed with KBr (195 mg) in a Thermo Nicolet 670 FTIR spectrometer equipped with a DTGS KBr detector in the range of 4000 cm^{-1} to 400 cm^{-1}, with 128 scan with a resolution of 4 cm^{-1}.

2.2 Photothermal Radiometry (PTR) System

A PTR system (Fig. 1) was used to study the thermal diffusivity of thermally treated bones. The sample is illuminated with a 100 mW modulated red (635 nm) laser diode

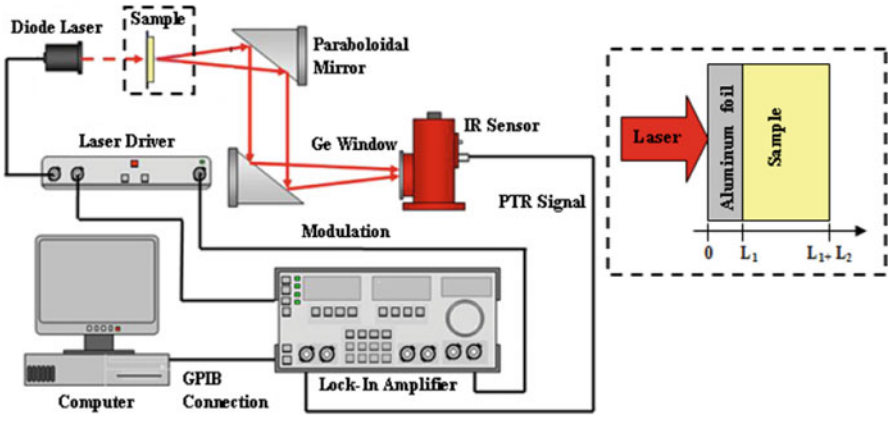

Fig. 1 PTR experimental setup system used to study thermally treated bones

beam, at a frequency f. As a consequence of the periodic heating of the laser, a train of modulated temperature changes (known as thermal waves) is generated in the sample. Due to this phenomenon, periodic infrared radiation is emitted by the sample surface, which is collected and focused onto a liquid N_2 cooled HgCdTe infrared detector, using two off-axis paraboloidal mirrors. The detector has an active area of $1\,mm^2$ and a sensitivity range between $2\,\mu m$ and $12\,\mu m$. The signal is pre-amplified (PA-300 Judson) before being sent into the lock-in amplifier (Stanford Research SR830). The amplifier outputs, amplitude and phase of the PT signal, are recorded as a function of the frequency. The amplifier only detects the signal at the modulation frequency, f, of the laser providing high control on the output signal. The penetration of the thermal wave inside the material is determined by the thermal diffusion length given by $\mu = \sqrt{\alpha/\pi f}$, where α is the thermal diffusivity [25].

The geometry of the studied system is shown on the right side of Fig. 1. It consisted of a sample of thickness L_2, thermal diffusivity α_2, and thermal conductivity k_2. The sample has an aluminum foil ($25\,\mu m$), with thermal diffusivity α_1 and thermal conductivity k_1, attached to it. The experiments were performed in forward scattering modality, in which the modulated laser light illuminates the aluminum substrate and the detection of the periodic radiation emitted by the sample is registered on the opposite surface. It has been shown that this procedure is useful in measuring the thermal diffusivity, since in this case the thermal wave transmission is monitored [25,26]. The amplitude of the modulated temperature at the surface of the sample is given by

$$T(L_1 + L_2) = \frac{2\eta\,(1-R)\,I_0}{(\sigma_1 k_1 + \sigma_2 k_2)}\left[\frac{e^{-\sigma_1 L_1} e^{-\sigma_2 L_2}}{1 + \Gamma(e^{-2\sigma_2 L_2} - e^{-2\sigma_1 L_1}) - e^{-2\sigma_2 L_2} e^{-2\sigma_1 L_1}}\right], \quad (1)$$

where $\Gamma = 1 - e_2/e_1$, $\sigma_n = (1+\mathrm{i})/\mu_n$, and $\mu_n = \sqrt{\alpha_n/\pi f}$ is the thermal diffusion length of aluminum foil ($n = 1$) and sample ($n = 2$). R is the reflectivity of the irradiated sample surface, η is the optical-to-thermal (nonradiative) energy conversion efficiency, and I_0 is the intensity of the illuminating beam. $e_1(\alpha_1)$ and $e_2(\alpha_2)$ are the thermal effusivities (thermal diffusivity) of the aluminum foil and sample, respectively.

When the thickness of the aluminum is small, in such a way that its thermal diffusion length μ_1, is at least two times greater than its thickness $\mu_1 > 2L_1$, it is said that it is thermally thin [27]. In this case in Eq. 1, the approximation $e^{-2\sigma_1 L_1} \approx 1$ can be performed [27]. On the other hand, if the thermal diffusion length μ_2 of the sample is smaller than half its thickness ($\mu_2 < L_2/2$), it is said that the sample is thermally thick, and the approximation $e^{-2\sigma_2 L_2} << 1$ can be used. It is important to mention that the thermally thin and thermally thick definitions used here are more strict that those currently used and discussed by Salazar et al. [27]. This more restrictive option was imposed to make sure that the specific thermal regime is adequate to analyze the experimental data, with the intention of obtaining a reliable characterization of a non-homogeneous material such as bone.

For a thermally thick sample and assuming that the aluminum foil is much thinner than the sample, the thermal-wave amplitude is given by

$$T(L_1 + L_2) = T(L_2) = \frac{(1 - R)\eta I_0}{e_2\sqrt{2\pi}} \frac{\mathrm{e}^{-L_2/\mu_2}}{\sqrt{f}}. \tag{2}$$

The temperature, given by Eq. 2, not only depends on the thermal diffusivity of the sample, but it is also inversely proportional to the thermal effusivity of the sample.

Additionally, for the thermally thick sample, the phase lag of the PTR signal dependence is given by

$$\varphi(L_2) = -\sqrt{\frac{\pi f}{\alpha_2}} L_2 + \varphi_0, \tag{3}$$

where φ_0 is a constant.

Performing a frequency scan, it is possible to determine the thermal diffusivity of the sample with

$$\alpha_2 = (L_2/m)^2\pi, \tag{4}$$

where m is the slope of the linear fit of phase experimental data as a function of the square root of the frequency.

In order to obtain thermal-diffusivity measurements, independent of the instrumental response of the specific PTR system, a calibration of the system frequency response was obtained using a thick glassy carbon sample (Sigradur). The PTR signal phase of the bone samples was normalized with respect to the reference of the glassy carbon in the range from 3 Hz to 23 Hz.

It is important to mention that the samples show microporosity, and therefore a partial absorption of thermal paste could be expected. In order to evaluate the influence of this factor, after each PTR experiment the aluminum foil was removed, the sample was cleaned, and a new aluminum foil was attached to it. This process was repeated three times for each sample, and the obtained data did not show any observable difference due to the absorbed thermal paste.

2.3 Diffuse Reflectance System

The diffuse reflectance system consists of a tungsten–halogen lamp that illuminates the sample using an optical fiber; the light reflected by the sample is collected using an integrating sphere (Labsphere USRS-99-010) and sent via a second optical fiber into a spectrometer (Ava Spec 2048). Spectra were recorded in the range from 400 nm to 800 nm. In order to normalize our measurements, a diffuse reflectance standard (Ocean Optics WS-1-SL) was used. The measurements were repeated three times for each sample, and an average of the obtained spectra was performed.

3 Results and Discussion

X-ray diffraction patterns of the powdered samples (Fig. 2a) of the non-thermally treated specimen (labeled as 25 °C) show broad peaks of HA structure. The shape of the main peak for 30° to 35° (2θ) is composed of four overlapping reflection lines (211), (112), (300), (202), and its intensity changes with thermal treatment as can be seen in sharp and well-defined peaks of the powder pattern at 800 °C. The relative intensity initially increases up to 250 °C and afterward diminishes (inset of Fig. 2a). This behavior is due to the contributions from both small size crystallites and micro-strains, indicating extensive lattice disorder due to the non-long-range order crystalline nature of the bone mineral [28]. The increase in the reflection peaks is due to a preferential resorption of smaller crystallites that could be interpreted as crystallite growth, although no actual crystal growth occurs [4].

The infrared spectrum (Fig. 2b) shows the corresponding bands of $[PO_4]^{3-}$ ions, a strong band composed of three stretching ($\nu 2$) modes ((1040, 1055, and 1079) cm^{-1}), a vibration mode at 961 cm^{-1} ($\nu 1$), and two bending modes ($\nu 3$) at 564 cm^{-1} and 604 cm^{-1}. For the $[CO_3]^{2-}$ ion, three vibration modes at 1063 cm^{-1}($\nu 1$), 874 cm^{-1}($\nu 2$), and 1415 cm^{-1} ($\nu 3$) are present. The band at 1751 cm^{-1} indicates the presence of carbonates at the channel sites in the structure [29]. Additionally, bioapatite shows a wide band from 3300 cm^{-1} up to 3600 cm^{-1} related to the OH stretching mode. The organic part vibrations from the amides appear in the region of 1511 cm^{-1} and 1657 cm^{-1}, and the bands at 2855 cm^{-1} and 2928 cm^{-1} belong to CH_2 and CH_3 [29].

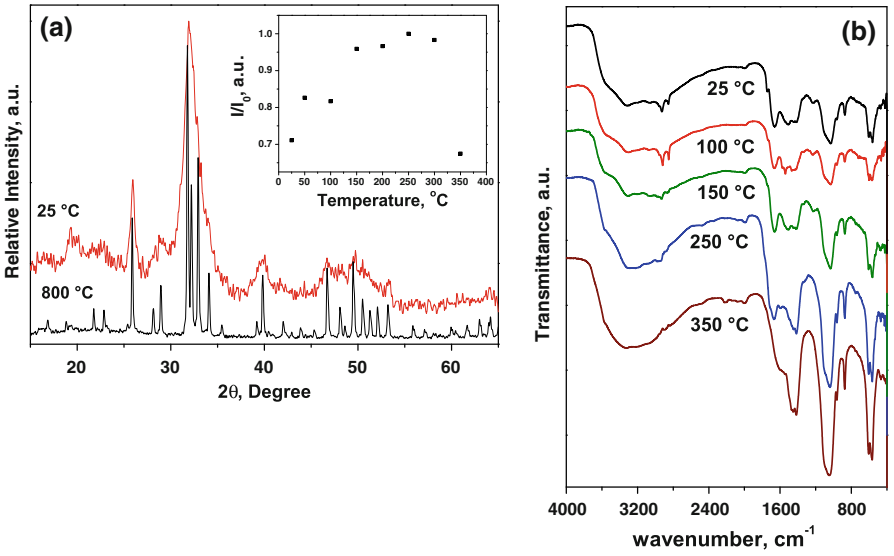

Fig. 2 (**a**) X-ray diffraction patterns of bone at room temperature and at 800 °C. The broad main peak at 30° to 35° (2θ) is composed of four overlapping reflection lines (211), (112), (300), (202), as can be seen in the 800 °C diffractogram. The *inset* shows the ratio in intensity of the peak at the interval from 30° to 35° (2θ) of diffractograms for thermally treated bones with respect to the 250 °C sample in the same interval and (**b**) FTIR spectra of the thermally treated bones

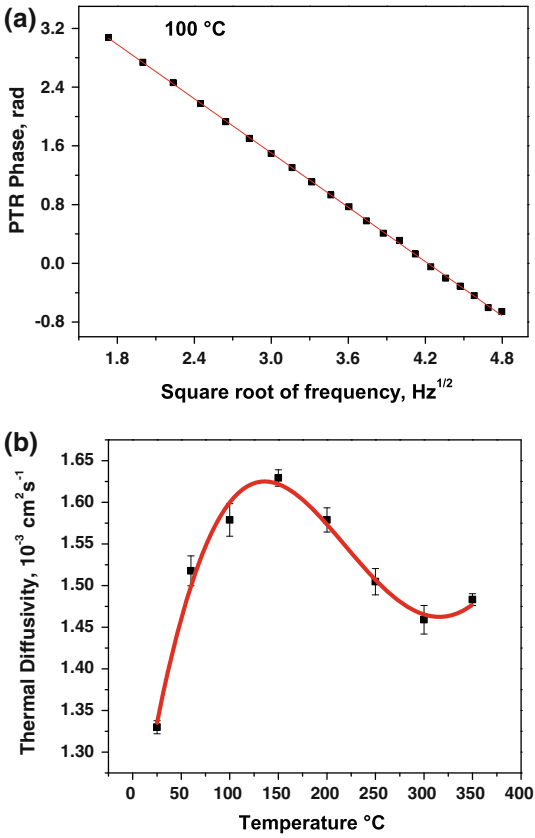

Fig. 3 (**a**) Experimental PTR signal phase as a function of the modulation frequency for a sample treated at 100 °C and (**b**) thermal diffusivity as a function of temperature for thermally treated bones

Several features in the infrared spectra, due to the thermal treatment, can be detected. A successive increase of the intensity of several PO_4 bands, at (1040, 1055, 1079, 564, and 604) cm^{-1} is observed. Also, the 1415 cm^{-1} and 874 cm^{-1} CO_3 bands increase, the latter attributed to a labile carbonate that in this case substitutes phosphate ions. On the other hand, the 1751 cm^{-1} band, related to the presence of carbonate at the channel sites, disappears above 100 °C [29]. It has been suggested that the disordered orientation of CO_3 in the OH channel generates diminution of OH bands and the broadening of CO_3 bands. This implies that the ordered degree of the channel ions increases smoothly after calcination below 150 °C [30]. Finally, the disappearance of CH_3 and CH_2 groups is observed above 100 °C, along with a progressive decrease in intensity in amide groups (1657 cm^{-1} and 1511 cm^{-1}), related to collagen decomposition and denaturing, respectively.

The thermal diffusivities of the bone samples were obtained from the fit of experimental phase data of the photothermal signal as a function of frequency applying Eqs. 3 and 4. As a typical example, in Fig. 3a the phase of the signal for a sample thermally treated at 100 °C is shown. In this case, the measured thermal diffusivity at room temperature was 1.34×10^{-3} $cm^2 \cdot s^{-1}$. The data of the thermal diffusivity for all the samples are presented in Fig. 3b. Upon heating, the thermal diffusivity increases

reaching a maximum around 130 °C ($1.62 \times 10^{-3}\,\mathrm{cm^2 \cdot s^{-1}}$); afterward, it shows a decay to $1.47 \times 10^{-3}\,\mathrm{cm^2 \cdot s^{-1}}$ at 325 °C. Experiments of the thermal properties for even higher temperatures could not be carried out due to the fragility of the samples. The behavior of the thermal diffusivity can be related initially to complex changes that occur in the bone, such as the elimination of material of low-thermal diffusivity through the release of water and the dehydroxylation process, and to mineral recrystallization. These effects can be observed by DRX and FTIR. With further heating, the organic material is degraded and/or eliminated, as the FTIR spectra exhibit [30], originating a diminution of the thermal diffusion.

It is important to stress that the thermal model being used for the photothermal characterization (See Eq. 1) is only adequate for homogeneous materials [25–27]. This is an important restriction in the thermophysical analysis of materials, especially those with important heterogeneities. In our case, considering that the hardest and most compact part of the bone is studied, the assumption, implicit in Eq. 1, can be considered to be suitable taking into account that the determined thermal diffusivity must be considered as an effective thermal property.

Thermal diffusivity studies for bone have been reported for cortical and spongy bovine samples and human cortical for studies of laser drilling [31]. Our results for the thermal diffusivity are in agreement with the human cortical thermal diffusivity [31]. Interestingly, the reported values for the thermal properties are close to those measured for samples made of nanostructured HA obtained from fish waste bones [32]. In this case, the powders were heated at 900 °C, compacted at a fixed pressure, and sintered at 1000 °C. Thermophysical properties were analyzed by thermal wave interferometry, and it was found that the thermal diffusivity increases as a function of milling time. A similar photothermal technique was successfully used to study HA coatings of commercial prosthetic hip stems [33]. Additionally, it has been shown that the thermal diffusivity of human enamel is higher than in bones, a result that should be expected taking into account that enamel is a ceramic-like HA material [34,35]. In contrast, in the case of human dentin, having a high porosity, lower values around $2.3 \times 10^{-3}\,\mathrm{cm^2 \cdot s^{-1}}$ have been reported [34–37]. These results indicate that the microstructure and composition are key factors in thermal diffusion; however, the detailed process of heat transport in non-homogenous materials and its effect on the macroscopic thermal properties is a subject that continues to be developed [38].

Diffuse reflectance in the visible region of the optic spectra, in the range from 400 nm up to 800 nm, is shown in Fig. 4a. These spectra show strong changes with thermal treatments. In order to better appreciate the temperature effects, the reflectance at 500 nm was plotted as a function of heating. It can be observed that the magnitude of the reflectance increases, reaching a maximum around 125 °C (inset of Fig. 4a). Above this temperature, the reflectance decays to values much lower than the ones obtained for ambient temperature, showing a partial stabilization at 300 °C.

Using the Kubelka–Munk approach, the quotient of the absorbance and the scattering $F(R)$ has been determined (Fig. 4b) [21]. It has been shown that $F(R)$ depends on the sample color and appearance related with the particle size. In all the temperature range, $F(R)$ shows a higher value for shorter wavelengths. When the temperature increases from 25 °C up to 150 °C, it can be observed by visual inspection that the sample exhibits a pale yellow color. For higher temperatures, the organic species begin

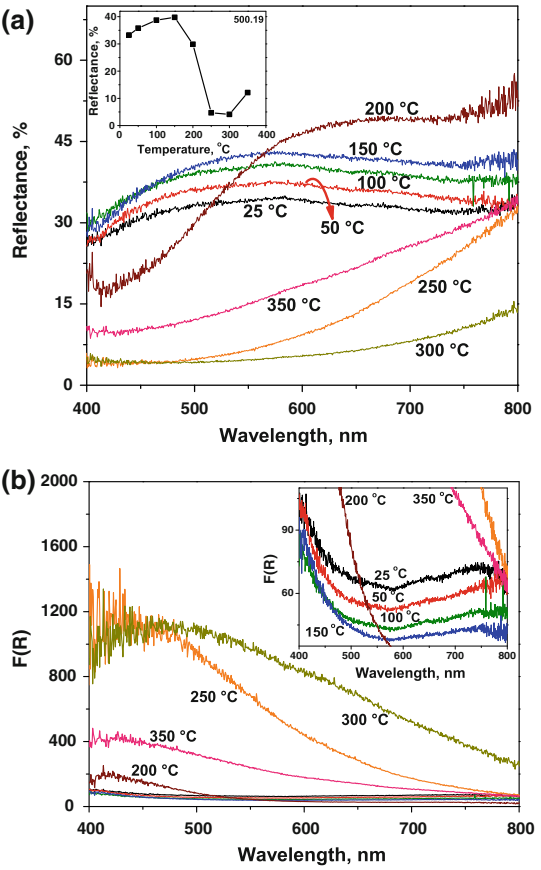

Fig. 4 (**a**) Reflectance curve and (**b**) quotient of the absorption with the scattering ($F(R)$) at different wavelengths of thermally treated bones. The *inset* in (**a**) shows the behavior of reflectance at 500 nm as a function of the temperature and the *inset* in (**b**) displays the curve for $F(R)$ from 25 °C up to 150 °C

to be burned; consequently at 300 °C, $F(R)$ reaches a maximum due to the oxidization of organic carbon with loss of mass and becomes dark brown at 350 °C [39].

The behavior of the optical and thermal properties can be understood based on the XRD and FTIR analysis. As discussed above, the increase of the main diffraction peaks is due to the release of microstrains in the lattice at short-order range [28]. Additionally, a preferential resorption of smaller crystallites is favored, although proper crystal growth does not occur [4]. From the FTIR results, it can be observed that below 150 °C, the disappearance of CH_3 and CH_2 groups and a progressive decrease in intensity in amide groups are related to collagen decomposition and denaturing. Therefore, the partial crystal reorganization and elimination of the organic low diffusivity material induces an increase in thermal diffusion and reflectance (at 500 nm).

Similar behavior has been observed in calcium carbonate for biogenic aragonite of Strombus gigas shells [40–42]. In this case, a glass transition around 180 °C in the organic matrix has been found when analyzing the role of the organic phase of the shell in crack propagation [40]. In the case of bones, our results would be a motivation to perform similar studies of the mechanical properties of bones during heating.

At higher temperatures, the XRD patterns and FTIR spectra indicate that the collagen is progressively degraded and induces a decrease in thermal diffusion and reflectance. On the other hand, the color changes in the thermally treated bones [39], from pale yellow changing to brown at 250 °C, are due to the combustion of the organic matter, reaching a strong darkening color at 350 °C due to carbonization. These color variations are in good agreement with the behavior of the absorbance-scattering ratio $F(R)$.

4 Conclusions

Photothermal radiometry and diffuse reflectance were applied to study thermal and optical properties of porcine thermally treated bone. Thin longitudinal bone sections were analyzed from room temperature up to 350 °C. The samples were structurally characterized by XRD and infrared spectroscopy. The thermal diffusivity and reflectance show an increase for the low-temperature range up to a maximum around 125 °C, and they decay at higher temperatures. Above this temperature, the thermal diffusion diminishes and the reflectance exhibits a strong decay to values much lower than the values found for samples at ambient temperature. It is shown that thermal diffusion and optical reflectance are sensitive parameters to detect complex changes in the biogenic composition, such as dehydration, dehydroxylation, elimination of the organic material, and removal of the fibril collagen networks, which have an influence on the bone chemical milieu and microcrystalline structural reorganization. The behavior of the absorbance-scattering coefficient mimics the color changes due to combustion and carbonization of the organic matter.

Acknowledgments This work was partially supported by the CONACYT on the projects 49275-F, Multidisciplinary-Cinvestav 2009, FOMIX 108160 and 108528, and the postdoctoral grant to S. Trujillo. The authors want to express their acknowledgments to M.S. J. Bante and M.S. D. Aguilar for their valuable help in the experimental arrangements and development of electronic circuits.

References

1. M.E. Fleet, Biomaterials **30**, 1473 (2009)
2. C.N. Trueman, K. Privat, J. Field, Palaeogeogr. Palaeoclimatol. Palaeoecol. **266**, 160 (2008)
3. J.C. Hiller, T.H. Wess, J. Archaoelog. Sci. **33**, 560 (2006)
4. K.D. Rogers, P. Daniels, Biomaterials **23**, 2577 (2002)
5. G. Piga, A. Malgosa, T.J.U. Thompson, S. Enzo, J. Archaeolog. Sci **35**, 2171 (2008)
6. S. Guizzardi, C. Montanari, S. Migliaccio, R. Strocchi, R. Solmi, D. Martini, A. Ruggeri, J. Biomed. Mater. Res. B Appl. Biomater. **53**, 227 (2000)
7. J. Catanese III, J. Featherstone, T. Keaveny, J. Biomed. Mater. Res. **45**, 327 (1999)
8. B. Yilbas, Z. Yilbas, M. Sami, Opt. Laser Technol. **28**, 513 (1996)
9. H. Pratisto, M. Frenz, M. Ith, V. Romano, D. Felix, R. Grossenbacher, H. Altermatt, H. Weber, Lasers Surg. Med. **18**, 100 (1996)
10. C.H. Hou, S.M. Hou, Y.S. Hsueh, J. Lin, H.Ch. Wu, F.H. Lin, Biomaterials **30**, 3956 (2009)
11. J.M. Very, R. Gilbert, B. Guilhot, M. Debout, C. Alexandre, Calcif. Tissue Int. **60**, 271 (1997)
12. N. Ugryumova, S.J. Matcher, D.P. Attenburrow, Phys. Med. Biol. **49**, 469 (2004)
13. E.A. Genina, A.N. Bashkatov, V.V. Tuchin, Proc. SPIE **6163**, 616311-1 (2007)
14. M. Heuret, C. Bissieux, L. Pincon, P. Egee, G. Kurka, J. Danroc, Surf. Coat. Technol. **45**, 325 (1991)
15. M. Heuret, E.V. Schel, M. Egee, R. Danjoux, Mater. Sci. Eng. B **5**, 119 (1990)

16. A. Gijsbertsen, D. Bicanic, J.L.W. Gielen, M. Chirtoc, Infrared Phys. Technol. **45**, 93 (2004)
17. C. Wang, A. Mandelis, NDT & E Int. **40**, 158 (2007)
18. V.P. Zharov, J.W. Kim, D.T. Curiel, M. Everts, Nanomed. Nanotechnol. Biol. Med. **1**, 326 (2005)
19. J.A. Garcia, L. Nicolaides, P. Park, A. Mandelis, B. Farahkbahsh, Anal. Sci. Special Issue **17**, s89 (2001)
20. E.S.R. Fonseca, M.E.P. de Jesus, Proc. SPIE **6631**, 66310C (2007)
21. M.G. Lagorio, J. Chem. Ed. **81**, 1607 (2004)
22. J.S. Dam, P.E. Andersen, T. Dalgaard, P.E. Fabricius, Appl. Opt. **37**, 772 (1998)
23. L. Perelman, V. Backman, M. Wallace, G. Zonios, R. Manoharan, A. Nusrat, S. Shields, M. Seiler, C. Lima, T. Hamano, I. Itzkan, J.V. Dam, J.M. Crawford, M.S. Field, Phys. Rev. Lett. **80**, 627 (1998)
24. S. Burch, A.J.M. Yee, in *Bone Metastasis: Experimental and Clinical Therapeutics*, ed. by G. Singh, S.A. Rabbani (Humana Press, Totowa, NJ, 2005), pp. 243–253
25. D. Almond, P. Patel, in *Photothermal Science and Techniques, Physics and its Applications*, ed. by E.R. Dobbs, S.B. Palmer (Chapman and Hall, London, UK, 1996)
26. A. Mandelis, P. Hess, in *Progress in Photothermal and Photoacoustic Science and Technology*, vol. III, Life and Earth Sciences (SPIE Optical Eng. Press, Bellingham, Washington, 1997)
27. A. Salazar, A. Sanchez-Lavega, J.M. Terron, J. Appl. Phys. **84**, 3031 (1998)
28. E.J. Wheeler, D. Lewis, Calcif. Tissue Res. **24**, 243 (1977)
29. A. Antonakos, E. Liarokapis, T. Leventouri, Biomaterials **28**, 3043 (2007)
30. Q.J. He, Z.L. Huang, X.K. Cheng, J. Yu, Mater. Lett. **62**, 539 (2008)
31. I.I.H. Chen, S. Saha, Ann. Biomed. Eng. **15**, 457 (1987)
32. T.M. Coelho, E.S. Nogueira, W.R. Weinand, W.M. Lima, A. Steimacher, A.N. Medina, M.L. Baesso, A.C. Bento, J. Appl. Phys. **101**, 084701 (2007)
33. A.C. Bento, D.P. Almond, S.R. Brown, I.G. Turner, J. Appl. Phys. **79**, 6848 (1996)
34. W.S. Brown, W.A. Dewey, H.R. Jacobs, J. Dent. Res. **49**, 752 (1970)
35. M. Braden, Arch. Oral Biol. **9**, 479 (1964)
36. T.A. El-Brolossy, S. Abdalla, O.E. Hassanein, S. Negm, H. Talaat, J. Phys. IV **125**, 685 (2005)
37. A.J. Panas, S.Z. Muda, J. Terpiłowski, M. Preiskorn, Int. J. Thermophys. **24**, 837 (2003)
38. S. Torquato, in *Random Heterogeneous Materials: Microstructure and Macroscopic Properties*, ed. by S.S. Antman, J.E. Marsden, L. Sirovich, S. Wiggins (Springer, New York, 2002)
39. L.E. Munro, F.J. Longstaffe, C.D. White, Palaeogeogr. Palaeoclimatol. Palaeoecol. **249**, 90 (2007)
40. S. Kamat, H. Kessler, R. Ballarini, M. Nassirou, A.H. Heuer, Acta Mater. **52**, 2395 (2004)
41. A. Hernandez-Ayala, P. Quintana, J.J. Alvarado-Gil, D. Aldana, J. Phys. IV **125**, 691 (2005)
42. J.J. Alvarado-Gil, P. Quintana, in *Thermal Wave Physics and Related Photothermal Techniques: Basic Principles and Recent Developments*, ed. by E. Marín-Morales (Transworld Research Network, Kerala, 2009), pp. 191–203